



MASTER'S THESIS

**Developing a Semi-Automatised Tool for
Grading Brain Tumours with
Susceptibility-Weighted MRI**

MARIA DUVALDT

August, 2015

Master's Thesis, Civilingenjörsprogrammet i teknisk fysik, Umeå University.
Maria Duvaldt, `madu0011@student.umu.se`.

Developing a Semi-Automatised Tool for Grading Brain Tumours with Susceptibility-Weighted MRI
is a project done in the course *Master's Thesis in Engineering Physics, 30.0 ECTS*
at the Department of Physics, Umeå University.

Supervisor: Tomas Jonsson, Karolinska University Hospital Huddinge.
Examiner: Jonna Wilén, Department of Radiation Physics, Umeå University.

Developing a Semi-Automatised Tool for Grading Brain Tumours with Susceptibility-Weighted MRI

Abstract

Gliomas are a common type of brain tumour and for the treatment of a patient it is important to determine the tumour's grade of malignancy. This is done today by a biopsy, a histopathological analysis of the tumourous tissue, that is classified by the World Health Organization on a malignancy scale from I to IV.

Recent studies have shown that the local image variance (LIV) and the intratumoural susceptibility signal (ITSS) in susceptibility-weighted MR images correlate to the tumour grade. This thesis project aims to develop a software program as aid for the radiologists when grading a glioma. The software should be able to separate the gliomas into low grade (I-II) and high grade (III-IV). The result is a graphical user interface written in Python 3.4.3. The user chooses an image, draws a region of interest and starts the analysis. The analyses implemented in the program are LIV and ITSS mentioned above, and the code can be extended to contain other types of analyses as research progresses.

To validate the image analysis, 16 patients with glioma grades confirmed by biopsy are included in the study. Their susceptibility-weighted MR images were analysed with respect to LIV and ITSS, and the outcome of those image analyses was tested versus the known grades of the patients.

No statistically significant difference could be seen between the high and the low grade group, in the case of LIV. This was probably due to hemorrhage and calcification, characteristic for some tumours and interpreted as blood vessels. Concerning ITSS a statistically significant difference could be seen between the high and the low grade group ($p < 0.02$). The sensitivity and specificity was 80% and 100% respectively. Among these 16 gliomas, 11 were astrocytic tumours and between low and high grade astrocytomas a statistically significant difference was shown. The degree of LIV was significantly different between the two groups ($p < 0.03$) and the sensitivity and specificity were 86% and 100% respectively. The degree of ITSS was significantly different between the two groups ($p < 0.04$) and the sensitivity and specificity were 86% and 100% respectively. Spearman correlation showed a correlation between LIV and tumour grade (for all gliomas $r = 0.53$ and $p < 0.04$, for astrocytomas $r = 0.84$ and $p < 0.01$). A correlation was also found between ITSS and tumour grade (for all gliomas $r = 0.69$ and $p < 0.01$, for astrocytomas $r = 0.63$ and $p < 0.04$). The results indicate that SWI is useful for distinguishing between high and low grade astrocytoma with 1.5T imaging within this cohort. It also seems possible to distinguish between high and low grade glioma with ITSS.

Keywords: Glioma grading, astrocytoma, susceptibility-weighted imaging, SWI, local image variance, intratumoural susceptibility signal, ITSS.

Utveckling av ett semi-automatiserat verktyg som stöd vid gradering av tumörer med hjälp av susceptibilitetsviktade MR-sekvenser

Sammanfattning

Gliom är en vanlig typ av hjärntumör och för patientens behandling är det viktigt att ta reda på tumörens malignitet. Detta görs idag genom en biopsi, ett vävnadsprov som analyseras mikroskopiskt och sedan klassificeras enligt en malignitetsgrad från I till IV.

Ny forskning visar att den lokala variansen i bilden (local image variance, LIV) och susceptibilitetssignalen i tumören (intratumoural susceptibility signal, ITSS) korrelerar till tumörens grad. Det här examensarbetet är gjort för att utveckla ett datorprogram som kan hjälpa till med graderingen av dessa tumörer, enligt forskning som tidigare gjorts. Med hjälp av bildanalys ska datorprogrammet kunna separera låggradiga tumörer (grad I-II) ifrån höggradiga (grad III-IV). Resultatet är ett grafiskt gränssnitt skrivet i Python 3.4.3, där användaren kan öppna en bild, rita ut ett intressant område och sedan starta bildanalysen. De implementerade analyserna är LIV och ITSS men programmet kan utvidgas för andra typer av bildanalyser efter intresse.

16 patienter med gliom vars grad redan säkerställts med biopsi var med i studien för att validera metoden. Deras susceptibilitetsviktade MR-bilder analyserades med avseende på LIV och ITSS. Resultaten från bildanalysen jämfördes sedan med patientens sanna grad från biopsin.

Ingen statistiskt signifikant skillnad kunde säkerställas mellan den höggradiga och den låggradiga gruppen vid analysen av LIV. Detta antagligen på grund av blödningar och förkalkning som är karkatäristiskt för vissa tumörer och misstas för blodkärl. För analysen av ITSS kunde en statistiskt signifikant skillnad säkerställas mellan de två grupperna ($p < 0.02$). Sensitiviteten och specificiteten var 80% respektive 100%. 11 tumörer var astrocytom och bland dem kunde höggradiga skiljas från låggradiga tumörer vid båda analyserna. Den lokala bildvariansen skilde sig i det fallet åt signifikant mellan de två grupperna ($p < 0.02$). Sensitiviteten och specificiteten var 86% respektive 100%. Nivån av ITSS skilde sig också åt signifikant i de två grupperna ($p < 0.04$) och sensitiviteten och specificiteten var 86% respektive 100%. Spearman korrelation visade ett signifikant samband mellan LIV och tumörgrad ($r = 0.53$, $p < 0.04$ för alla gliom och $r = 0.84$, $p < 0.01$ för astrocytom). Det fanns även en signifikant korrelation mellan ITSS och tumörgrad ($r = 0.69$, $p < 0.01$ för alla gliom och $r = 0.63$, $p < 0.04$ för astrocytom). Resultaten visar att susceptibilitetsviktade MR-bilder tagna vid 1.5T kan användas för att skilja på låg- och höggradiga astrocytom i denna kohort. Det är även möjligt att skilja på låg- och höggradiga gliom genom att titta på ITSS.

Contents

1	Introduction	1
1.1	Background	1
1.2	Aim	1
1.3	Goal	1
1.4	Limitations	2
1.5	Disposition	2
2	Theory	3
2.1	Introduction to Tumours	3
2.2	Magnetic Resonance Imaging	4
2.3	Susceptibility-Weighted Imaging	6
2.4	Analysing the Local Image Variance	6
2.5	Analysing Intratumoural Susceptibility Signal	9
2.6	Specificity and Sensitivity	9
3	Method	11
3.1	Program	11
3.2	Patients	11
3.3	Imaging Parameters	11
3.4	Image Analysis	12
3.5	Statistical Analysis	12
4	Results	13
4.1	Program Description	13
4.2	Algorithm Description	16
4.3	Analysing Local Image Variance	16
4.4	Intratumoural Susceptibility Signal	20
5	Discussion	24
5.1	The Program	24
5.2	Filtering	24
5.3	Local Image Variance	25
5.4	Intratumoural Susceptibility Signal	26
5.5	General	26
5.6	Future	27
6	Conclusion	28
7	Bibliography	29

Chapter 1

Introduction

This chapter serves as an introduction to the problem formulation of the master's thesis. The background section briefly presents the research that has led towards this project and explains why it is needed. The aim and goal of the project are clearly stated, as well as the limitations of the project.

1.1 Background

Gliomas represent the majority of malignant brain tumours in adults. An important feature in planning the treatment of the patient is the grading of the glioma. The grade is a label on how malignant the tumour is and the scale is set by World Health Organization (WHO) from I to IV where IV is the most malignant.[1] The WHO grade is determined by a biopsy, investigating a tissue sample of the tumour microscopically.

Magnetic resonance imaging, or MRI, is the modality of choice for evaluating patients who show signs of a brain tumour. It has superior soft tissue resolution and is very useful for assessing tumour location and extent, and planning further treatment of the patient [2]. Since MRI is a relatively new technique, new protocols and sequences are continuously developed and proposals of new applications are published every year. Susceptibility-weighted imaging, or SWI, is a protocol that uses the magnetic properties of blood to image veins and hemorrhage [3]. It has been shown that the viability and aggressiveness of gliomas is correlated to a high production of blood vessels [4], and some studies suggest that the glioma grade might be possible to find by high-resolution imaging alone [4, 5, 6].

The study of local image variance in a 7T SWI image has been shown to significantly distinguish between the cases of high grade glioma (grade III-IV) and low grade glioma (grade I-II) [6]. Some studies use both the intratumoural susceptibility signal from SWI to calculate the amount of blood vessels within the tumours and perfusion-weighted imaging to successfully grade the tumours [4, 5, 7]. Ergo, these methods suggests that the grade can be determined in a non-invasive way, solely by analysing the SWI images. In that case a biopsy would not be needed and this would save effort for the patient, as well as resources at the hospital.

At Karolinska University Hospital Huddinge the SWI protocol has been introduced for brain tumours during the spring of 2015. The MR-physicists now wishes to implement a tool that by image analysis could help the radiologists to grade the gliomas.

1.2 Aim

The result of this project is a software that aims to assist the radiologists in determining whether a tumour is low grade (I-II) or high grade (III-IV) according to the WHO classification. This is a pilot project that in the long run might reduce the need of a biopsy. The patients would then benefit by not having to undergo the tissue sample procedure and the clinic might spend their resources elsewhere. The treatment could start directly and the patient would not have to spend time waiting for the biopsy. It is also a step on the way towards integrating the MR-physicists more into the clinical work.

1.3 Goal

There are two goals of the project. The first is a computer program with a graphical user interface (GUI) where a radiologist can open a DICOM image and draw a region of interest (ROI). The ROI should be saved and accessible for image analysis with any method of choice implemented in the software. A computer

program with well thought out structure is desired, since it hopefully will be further expanded to contain more types of image analyses.

The second goal of the project is to distinguish between high and low grade gliomas by image analysis only. This should be done with the computer program created. The ROI drawn in the image should be analysed with respect to the local image variance and the intratumoural susceptibility signal, two types of analyses that other research has shown correlate to tumour grade [6, 7]. To verify the method, 16 patients with glioma grade confirmed by biopsy are included in the study. The results of the image analyses will be tested versus the confirmed grades of these patients, and the outcome will show if the method is valid or not.

1.4 Limitations

The project is limited to gliomas at 1.5T. The study is retrospective so the parameters of the SWI protocol will not be the same as in the research studied. The number of patients is 16. The study is done with patients from Karolinska University Hospital Huddinge and Solna and Södersjukhuset.

1.5 Disposition

This thesis includes six sections, starting with this introduction. Section 2 contains the theory part, which introduces a few different subjects: tumours in general, gliomas in particular, MRI and SWI. The readers already familiar with medical physics are free to skip those parts, since the target group of this master thesis is students of engineering physics in general. The rest of the theory section contains the specific image analysis done and the statistical analysis. Section 3 describes the method, the patient cohort and the camera parameters used. The results in section 4 explain the written software and it's functions as well as state the results of the image analysing and tumour grading. In section 5 further suggestions and possible sources of uncertainty are discussed, and in section 6 the results are concluded.

Chapter 2

Theory

This section gives a brief introduction to a number of subjects, such as tumours, gliomas, WHO grading, magnetic resonance imaging and weighted imaging, needed to understand the project thoroughly. After that, the actual image analyses done in this project are explained. As already mentioned the target group is students of engineering physics, and the reader already familiar with medical physics can skip the first parts of the theory.

2.1 Introduction to Tumours

A tumour, or a neoplasm, is an abnormal growth of tissue that serves no physiological function. Tumours can be benign or malignant. A mole is an example of a benign tumour, it does not invade other tissue or metastasize. A malignant tumour is more prone to invade adjacent tissues and spread to other sites in the body by metastasizing [8]. Another word for malignant tumour is cancer. Tumours have different characteristics depending on which cell they evolve from. For example *lymphoma* is a group of blood cell tumours that develop from lymphatic cells, *gliomas* grow from glial cells usually in the brain or spine.

2.1.1 Gliomas

About 80% of all malignant brain tumours in adults are gliomas [1]. Each type of tumour occurs due to an abnormal cell growth of a specific cell type and the aggressiveness of these cells is an important feature for the treatment of the patient. Gliomas are classified by WHO on a malignancy scale based on histological features [9], meaning the microscopic anatomy of the tumourous tissue. This is done by taking a biopsy, a tissue sample, of the tumour and analysing it with a microscope. The grades are seen in table 2.1.

Table 2.1: *The WHO classification of brain tumours. [9]*

WHO grade	Description
I	Includes lesions with low proliferative potential, a frequently discrete nature, and the possibility of cure following surgical resection alone.
II	Includes lesions that are generally infiltrating and low in mitotic activity but recur. Some tumour types tend to progress to higher grades of malignancy.
III	Includes lesions with histologic evidence of malignancy, generally in the form of mitotic activity, clearly expressed infiltrative capabilities, and anaplasia.
IV	Includes lesions that are mitotically active, necrosis-prone, and generally associated with a rapid preoperative and postoperative evolution of disease.

A few examples of types of gliomas, grades, prevalence and survival rates can be seen in table below. A five-year survival rate is a measurement of how many patients that are alive five year after the point of diagnosis.

Table 2.2: Examples of gliomas, grades and survival rates. [1, 10]

Glioma	WHO grade	Prevalence	Five-year survival rate
Diffuse astrocytoma	II	1.6% of all gliomas	47.4%
Oligodendroglioma	II - III	6.5% of all gliomas	80%
Anaplastic astrocytoma	III	6.7% of all gliomas	27.3%
Glioblastoma	IV	55% of all gliomas	5.0%

Astrocytoma account for 80% of all gliomas and grow from a special kind of glial cells called astrocytes [9]. Oligodendrogliomas are a type of glioma that grow from oligodendrocytes in the brain. Oligodendrogliomas are typically calcified which can be identified on unenhanced CT-images. The patients included in this project have tumours shown in table 2.2. A feature of a malignant glioma is the production of new blood vessels, angiogenesis, which has been shown to be associated with tumoural aggressiveness and viability, and thus with the grade of the glioma [4].

2.2 Magnetic Resonance Imaging

The signal measured in magnetic resonance imaging, or *MRI*, comes from a hydrogen nucleus consisting of a single positively charged proton. Water and fat contains a lot of hydrogen, and this is used for imaging the human body, since the body consists to most part of water and fat. The proton spins around its own axis and this spinning charge creates a current which generates a small magnetic field, a magnetic moment.[11] If the proton is placed in an external magnetic field as B_0 in figure 2.1 it experiences a torque and tries to align itself with the external field. However the laws of quantum mechanics restricts the proton from aligning exactly and it continues to experience a torque which makes it precess around the direction of the field, with a frequency proportional to the external magnetic field, the Larmor frequency.[11] There are many protons and in the transversal plane they are all out of phase with each other during equilibrium. In the direction of the external field B_0 the protons pointing upward are slightly over-represented and a vector sum of all these magnetizations will therefore be in the direction of the field. This is called the net magnetization and it can be seen in figure 2.2. [11]

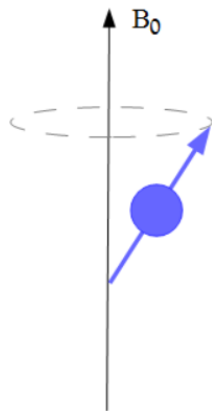


Figure 2.1: Proton precesses around the main magnetic field B_0 .

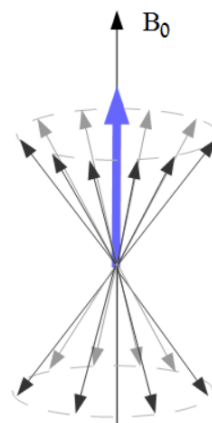


Figure 2.2: The net magnetization (along the direction of B_0) from averaging many protons.

Using a radiofrequent pulse (RF pulse) of the Larmor frequency, the net magnetization is tipped into the transversal plane, as in figure 2.3. This RF pulse also brings the spins into a phase coherence. When the RF pulse is switched off the protons begin to relax back to equilibrium position again. This is done in two ways, a dephasing of the spins in the transversal plan as well as a realignment along the z-axis. The

first effect is called *spin-spin relaxation* and is measured as T_2 . It can be seen in figure 2.4. The second relaxation effect is the *spin-lattice relaxation*. It is measured as T_1 and seen in figure 2.5. These relaxation mechanisms decrease the magnetization, which is the signal we detect in MRI. T_1 and T_2 changes with field strength and in human tissues T_1 is always larger than T_2 . [11]

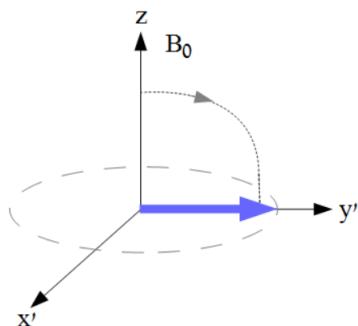


Figure 2.3: The net magnetization is tipped into the transversal plane.

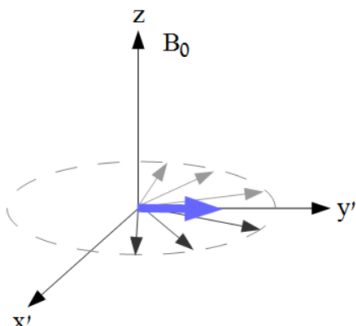


Figure 2.4: A dephasing due to spin-spin relaxation occurs.

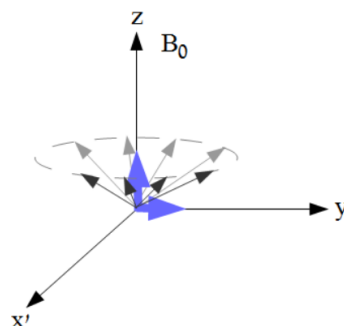


Figure 2.5: Spin-lattice relaxation realigns the magnetization along the z-axis.

The parameters T_1 and T_2 are of great importance in MRI for distinguishing different tissues. All MR images are produced using pulse sequences that contains radiofrequency pulses and also gradient pulses used for spatial encoding. The pulses are applied with very specific timing and duration. The echo time TE is the time from the application of the RF-pulse to the start of the acquisition. The repetition time TR is the time from the application of one excitation pulse to the application of the next one. There are many different pulse sequences and they all use these timing parameters TR and TE which can be modified. [11]

Common field strengths in clinical MRI is 1.5T or 3T, and there are scanners up to 11T for research purposes. The signal is proportional to the field strength and a higher field strength means more signal. The extra signal can be used to reduce the acquisition time or increase the resolution.

2.2.1 Weighting

The contrast of the images mainly depend on either T_1 , T_2 or proton density. In T_2 -weighted images tissues with long T_2 are bright. The sequences have a long TE and TR , and we look at the protons that stay longer in the transversal plane. Fluids have a high T_2 and get bright, water- and fat-based tissues appear mid-gray. T_1 -weighted images have a short TE and TR and show protons that relax rather quickly. Fluids get dark (unless they are flowing into the imaging volume), water-based tissues appear grey and fat-based tissues get bright. Figure 2.6 shows a T_1 and a T_2 weighted image of a brain. The ventricles with cerebrospinal fluid is dark in the T_1 -weighted image and bright in the T_2 -weighted image. Notice also the difference of the grey levels for the white and grey matter.

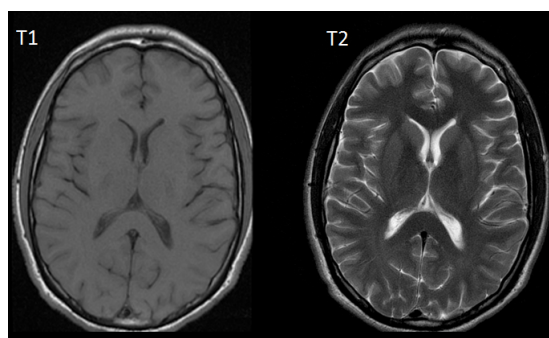


Figure 2.6: T_1 versus T_2 of an axial image of a brain. The ventricles with cerebrospinal fluid is bright in the T_2 -weighted image, while the bone surrounding the brain is dark and the white matter is grey. [12]

It is common to scan a patient with a couple of sequences designed for that particular problem formulation, pre-defined as a protocol. In addition to T_1 - and T_2 -weighting there are other sequences that enhance certain types of tissue. For example *FLAIR* (*FLuid Attenuated Inversion Recovery*) generates a T_2 -weighted image with suppressed signal from cerebrospinal fluid, and *STIR* (*Short TI Inversion Recovery*) is a fat-suppression sequence that gets a very low signal from fat but high signal from fluids. Another example of a MRI-technique is susceptibility-weighted imaging, or *SWI*, which is used in this project.

2.3 Susceptibility-Weighted Imaging

Magnetic susceptibility is the magnetic response of a substance when it is placed in an external magnetic field [13]. Susceptibility-weighted imaging, *SWI*, is a type of contrast different from T_1 and T_2 . *SWI* distinguishes any tissue that has different susceptibility than its surrounding structures, and produces images sensitive to venous vasculature, blood products (that occurs after hemorrhage) and changes in iron content. [3, 14] Small veins are paramagnetic since they have a high concentration of deoxyhemoglobin. This property works as an intrinsic contrast agent and induces a difference in magnetic susceptibility between the blood and surrounding tissues. Both paramagnetic (deoxyhemoglobin in blood) and diamagnetic (calcium) substances change the magnetic field. In the final susceptibility-weighted image they are both shown as hypointense. In figure 2.7 a T_2 - and a susceptibility-weighted image from a traumatic brain injury are shown. The arrows point at small hemorrhagic injuries in the white matter which are easier to distinguish with *SWI*.

An MR image is composed of two parts, a magnitude image of the signal and a phase image. *SWI* focuses on the phase image to measure small differences in the phase due to different magnetic susceptibilities of the tissues.

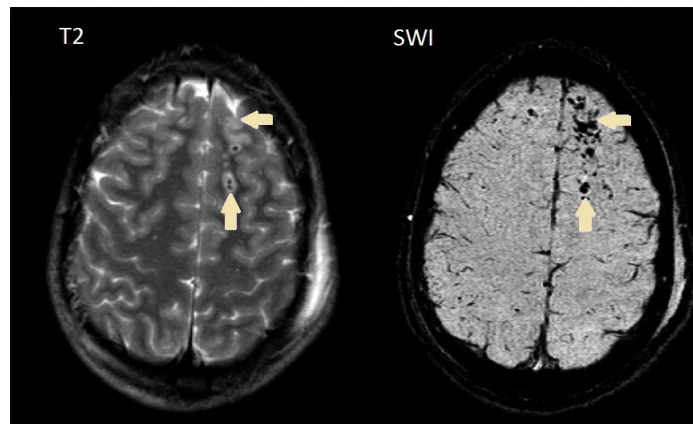


Figure 2.7: T_2 versus *SWI*. The small hemorrhagic injuries in the white matter are easier to distinguish with *SWI*. [15]

As mentioned in section 2.1.1, gliomas are known to have a high production of blood vessels and increased blood supply. It has been shown that the local variance within the tumour region in a susceptibility-weighted image could correspond to the aggressiveness of the tumour [6].

2.4 Analysing the Local Image Variance

In a greyscale image a pixel is represented by one value for the intensity of the shades of grey. The scale ranges from black at the weakest intensity to white at the strongest. Each pixel in an image is represented by a numeric value in this predefined range. Black is always represented by 0 and white is often 255 for a system that stores 8 bits per sampled pixel.

Grabner et al. have analysed glial tumours from susceptibility-weighted images at 7T and correlated the local image variance (*LIV*) to the glioma grade [6]. The expression for variance of an arbitrary variable

$V(X)$ from a sample is

$$V(X) = E[X^2] - E[X]^2 \quad (2.1)$$

where $E[X]$ signifies the expectation value of the variable X . In a 2D-image as figure 2.8, the local image variance for a pixel at position ij as the one inside the closed square in figure 2.8 becomes

$$V_{ij} = \frac{1}{(2L+1)^2} \sum_{k=i-L}^{i+L} \sum_{l=j-L}^{j+L} I_{kl}^2 - \left(\frac{1}{(2L+1)^2} \sum_{k=i-L}^{i+L} \sum_{l=j-L}^{j+L} I_{kl} \right)^2 \quad (2.2)$$

where I_{kl} is the pixel intensity at the position kl . L is an arbitrary number of pixels determining the size of the area over which we average. The dashed square represents the area $(2L+1)^2$ in the denominator of equation 2.2.

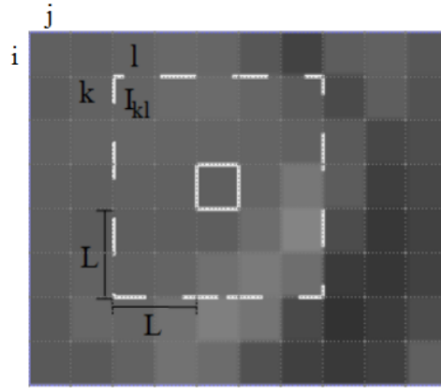


Figure 2.8: The closed white square represents the pixel that the local image variance is calculated for. The dashed square is the area with pixels that contributes to the averaging.

2.4.1 Filtering

A Gaussian filter is a low pass filter that reduces the high frequency components of the image. It also reduces image noise and detail.

The area chosen as denominator of equation 2.2 in the analysis of Grabner et al. [6] was a Gaussian filter kernel with a full width at half maximum, $FWHM$, of 3mm. For a normal distribution, the relationship between the $FWHM$ and the standard deviation σ is derived below. Consider a normal distribution seen in figure 2.9 on the form

$$f(x) = \frac{1}{\sigma\sqrt{2\pi}} \exp\left[-\frac{(x-x_0)^2}{2\sigma^2}\right] \quad (2.3)$$

where x_0 is an arbitrary value. The $FWHM$ is found where $f(x)$ reaches half of its maximum value. The maximal height of the peak, f_{max} , occurs at $f(x_0)$, that is

$$f_{max} = f(x_0) = \frac{1}{\sigma\sqrt{2\pi}} \exp\left[-\frac{(x_0-x_0)^2}{2\sigma^2}\right] = \frac{1}{\sigma\sqrt{2\pi}}. \quad (2.4)$$

Thus, at the half of f_{max} we get the relation

$$\frac{1}{2} \frac{1}{\sigma\sqrt{2\pi}} = \frac{1}{\sigma\sqrt{2\pi}} \exp\left[-\frac{(x-x_0)^2}{2\sigma^2}\right]. \quad (2.5)$$

Solving for x we obtain

$$x_{1,2} = \pm \left(\sigma\sqrt{2\log 2} + x_0 \right) \quad (2.6)$$

and as $FWHM$ is given by subtracting one point from the other, as can be clearly seen in figure 2.9.

$$FWHM = 2\sigma\sqrt{2\log 2} \approx 2.35\sigma. \quad (2.7)$$

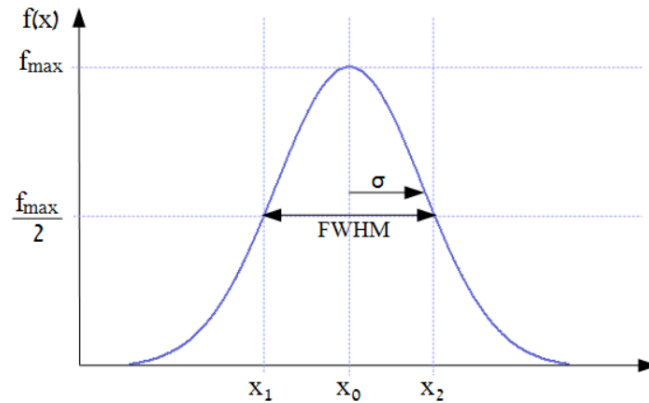


Figure 2.9: The full width at half maximum, $FWHM$, and σ of a normal distribution.

2.4.1.1 Filter Parameters

The standard deviation σ is a measurement of the sharpness of the peak in the Gaussian bell shape. It is seen in figure 2.9 and 2.10. A larger σ results in broader peak and, when filtering an image, puts more weight on the adjacent pixels as seen in 2.10.

Truncation means that a value has to be cut off at an integer step. The truncation for the filter tells how many pixels we choose to consider when doing the weighting. The Gaussian curve expressed in 2.3 reaches zero at infinity but the number of pixels used to get a weighted mean of each element need to be finite, truncated at some appropriate value. In figure 2.10 the dashed vertical lines represents the pixels. The central element that should be analysed (marked c) is in the middle. The whole image consists of seven pixels, three on each side of the central element. A truncation of two pixels is highlighted by the black dashed lines. The horizontal dashed line show where the Gaussian curve intersects intersects the pixels edges. The relative weights are shown as w_c for the central element, w_1 for the first adjacent pixel, and w_2 for the next one. For $\sigma = 1.5$ the weight of the second pixel is about 10% of the weight of the central value, but for $\sigma = 5.0$ it is about 80%. So for different σ the relation between the weights are different, for a specific truncation. To have a truncation of more than three pixels would be unnecessary in the case of $\sigma = 1.5$ since the curve falls off quickly. So the truncation tells how many pixels that contribute to the average of our central element, and the standard deviation σ tells their weights.

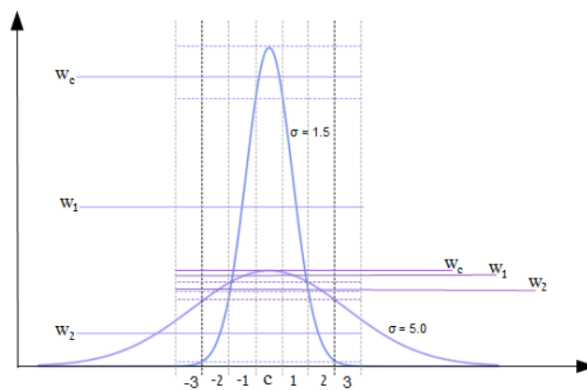


Figure 2.10: Illustration of how the truncation and σ affects the weights w_c, w_1, w_2 of the pixels in the analysis.

2.5 Analysing Intratumoural Susceptibility Signal

Intratumoural susceptibility signal or ITSS is defined as the "linear or dot-like low signal within the tumor", in the susceptibility-weighted images [5]. Studies have shown that the number of these structures within the tumour correlate significantly to tumour grade [4, 5]. In the studies mentioned, the structures were counted manually when evaluating the images. Calcification and macrohemorrhage (that also appear hypo-intense as mentioned in section 2.3) were excluded due to low signals in conventional MR and SWI phase imaging.

Another study of ITSS [7] evaluates the percentage of low-intensity pixels in the tumour region. The normalized contrast of each pixel in the ROI is calculated by

$$NC = \frac{\mu_{non-ITSS} - I_{SWI}}{STD_{NWM}}. \quad (2.8)$$

$\mu_{NON-ITSS}$ is the mean intensity of the non-ITSS pixels, which was estimated using the method of Otsu's threshold explained in section 2.5.1 below. I_{SWI} is the intensity of each pixel and STD_{NWM} is the standard deviation of a normal white matter region, which represents the signal fluctuation of SWI. Thus regions with low gray levels (suspected to be venous blood or hemorrhage) present high NC values. A fixed value of NC is set as a threshold and the number of pixels above that threshold represents the percentage of ITSS within the tumour. A high value would correlate to a high tumour grade. In this study a threshold for $NC > 10$ gave a significant result in differentiating low and high grade astrocytomas [7].

2.5.1 Otsu's method

Otsu's thresholding is a common method for dividing an image into two parts, to extract objects from their background. The image is assumed to have two classes of pixels, darker and brighter. The threshold between the two are calculated in order to minimize the spread within each of the classes [16]. An example of Otsu's thresholding and a division of the pixel classes is seen in figures 2.11 and 2.12 below.



Figure 2.11: Image before Otsu's thresholding.[17]



Figure 2.12: Image after Otsu's thresholding.[17]

2.6 Specificity and Sensitivity

The specificity and sensitivity are measurements of the diagnostic performance of a system, used for evaluating medical equipment. The decisions must be binary, for example a disease can be either present or absent.[18] An example is a diagnostic test where the question is if a person has a certain disease or not. The possible outcome can be seen in table 2.3 below. *True positive* occurs when the test is positive and the person has the disease, *false positive* is when the test indicates a disease but the person really is healthy. Analogically *false negative* occurs when the test suggests healthy but the person do have the disease and *true negative* is when the test is negative and the person is healthy.

Table 2.3: *An analysis of a test for a certain disease.*

		Disease in reality	
		Yes	No
Test	Yes	True positives (TP)	False positives (FP)
	No	False negatives (FN)	True negatives (TN)

The *sensitivity* of the system is defined by the true positive fraction TPF

$$TPF = \frac{n_{TP}}{n_{TP} + n_{FN}}, \quad (2.9)$$

where n_{TP} and n_{FN} are the number of true positive and false negative outcomes respectively. The *specificity* of the system is defined by the true negative fraction TNF

$$TNF = \frac{n_{TN}}{n_{TN} + n_{FP}}, \quad (2.10)$$

where n_{TN} and n_{FP} are the number of true negative and false positive outcomes respectively.

Chapter 3

Method

This section includes a description of how the model was elaborated, the patient cohort and the camera parameters used. The specifics of the tumour segmentation and the statistical analyses used are also explained.

3.1 Program

The program was written in *Python 3.4.3* with the editor *JetBrains PyCharm Community Edition 4.0.5*. The construction of the graphical user interface started from the user's point of view by reflecting on how a interface would look. A simple mind map which later turned into the callgraph (figure 4.1) is seen in figure 3.1. Other MR physicists, X-ray physicists and radiologists were questioned about the design and appearance of the features. The imaging analyses implemented were the mean local image variance (LIV) as it was done by Grabner et al. [6] and the intratumoural susceptibility signal (ITSS) with inspiration from Chuang et al. [7].

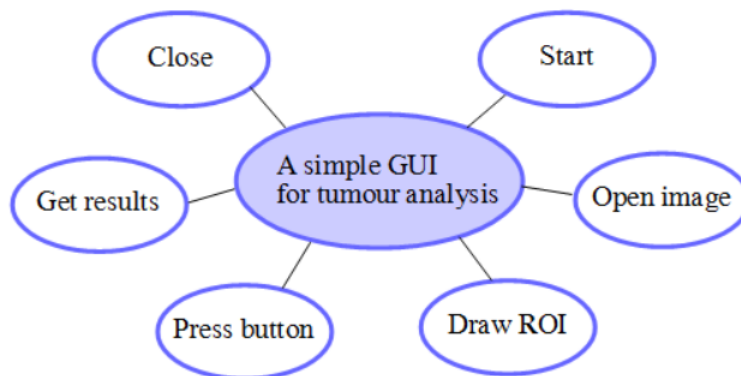


Figure 3.1: A mindmap of the user's perspective of the program.

3.2 Patients

16 patients in ages 23 to 86 were included in the study, 5 women and 11 men. 9 of the tumours were glioblastoma grade IV, 1 was anaplastic astrocytoma grade III and 1 was pleomorphic xanthoastrocytoma grade III. 2 tumours were oligodendrglioma grade II and 4 were astrocytoma of grade II.

3.3 Imaging Parameters

The scanning parameters are seen in table 3.1 below. All scanners were from Siemens and the images were reconstructed with Siemens software *Syngo MR*.

Table 3.1: *The parameters used in this study, all scanners from Siemens.*

Scanner	Aera	Avanto	SymphonyTim	TrioTim
Field strength (T)	1.5	1.5	1.5	3
TE (ms)	40	40	40	20
TR (ms)	49	49	50	28
Image matrix (pixels)	256 x 224	256 x 224	256 x 224	320 x 240
Resolution (mm)	0.86 x 0.86 x 2.0	0.90 x 0.90 x 2.0	0.90 x 0.90 x 2.0	0.72 x 0.72 x 1.6

3.4 Image Analysis

The grades were determined with a pathological anatomical analysis, a biopsy. The images were taken from SWI-examinations at Karolinska Huddinge and Södersjukhuset between 2012 and 2015. The tumour segmentation was performed by an experienced neuro-radiologist. The regions of interest were taken at the part of the tumour that seemed most malignant with respect to contrast enhancement in T_1 -weighted images, diffusion-weighted images and perfusion-weighted images.

The filter parameters were evaluated by varying σ from equation 2.7 between 1-5mm and truncation between 0.5-6 pixels. Since the goal was to separate the high grade (HG) from the low grade (LG) gliomas, an analysis of σ and truncation was done when looking at the mean of the two groups, $HG_{mean} - LG_{mean}$ and their combined standard deviation.

The threshold for the normalized contrast was varied between 0 and 100 to find the optimal value for grade differentiation in the ITSS-analysis.

3.5 Statistical Analysis

The Mann-Whitney test was used to evaluate the differentiation of the means of the two grades, for LIV and ITSS. The result was significant for $p < 0.05$. Spearman Correlation Coefficients were used to correlate the LIV and ITSS to the pathological grade. These tests were chosen since a normal distribution was not assumed. The statistical analysis was done with Python 3.4.3. and the NumPy and SciPy packages. Binary logistics (specificity and sensitivity) were used to compute the efficiency of grading the tumours in this study.

Chapter 4

Results

The results of the project are divided into two parts presented here. The first one consists of the actual software created. A presentation of the libraries used is given and pseudo code explains the algorithms. The second part describes the outcome of the image analyses.

4.1 Program Description

The code has been written in *Python 3.4.3*. *Python* uses a lot of libraries with in-built functions, of which a few will be described here.

Figure 4.1 shows the call graph for the program called *Tumour Analysis Tool*. `Main()` is an infinite loop executed when the program runs and `Draw()` is also run in that loop. The filled purple boxes in the picture represents the activities controlled by the user by buttons in the graphical user interface (GUI).

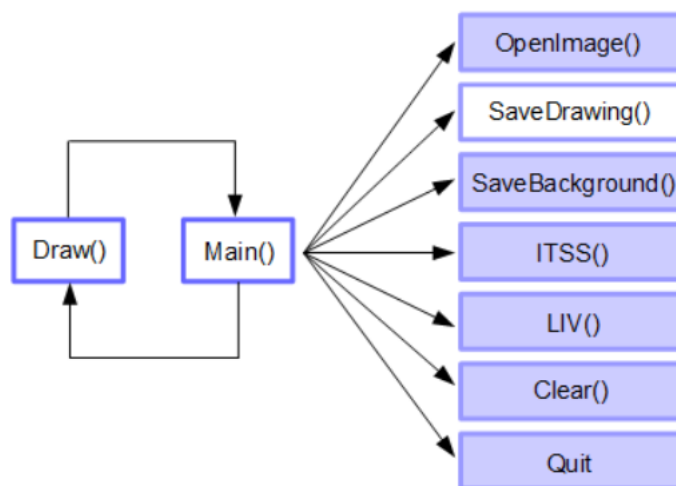


Figure 4.1: *The call graph for the program.*

When running the program and `Main()` the window in figure 4.2 is displayed. The buttons are seen in the top row. When pressing `Open image` a file directory dialogue box is opened and the user chooses the appropriate DICOM-image. This is seen in figure 4.3. By holding down the left mouse button the user then draws a background region somewhere in the image, for example in the top left corner, and presses `Background` as in figure 4.4. The user then draws a region of interest somewhere in the image, as in 4.5. With a region chosen the user presses one of the analysis-buttons. Pressing `LIV` calls the local image variance analysis and displays the result as seen in figure 4.6. To clear the coloured region of interest and the LIV presented the user presses `Clear`. To do the ITSS analysis the user presses `ITSS`. The analysis is performed and the result is displayed as in figure 4.7. Each activity is executed from `Main()` and the loop runs until the user presses `Quit`.

CHAPTER 4. RESULTS

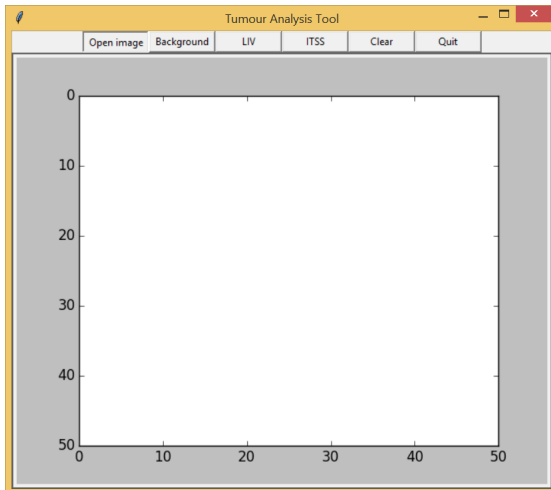


Figure 4.2: The program starts and the user presses *Open image*.

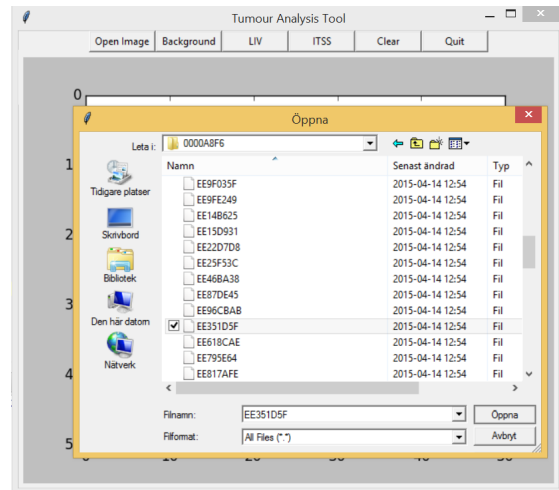


Figure 4.3: A file directory opens and the user chooses an image and presses *Öppna*.

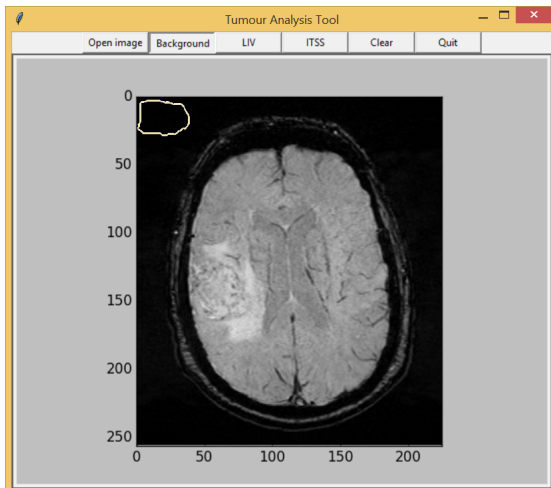


Figure 4.4: The user draws a background region and presses *Background*.

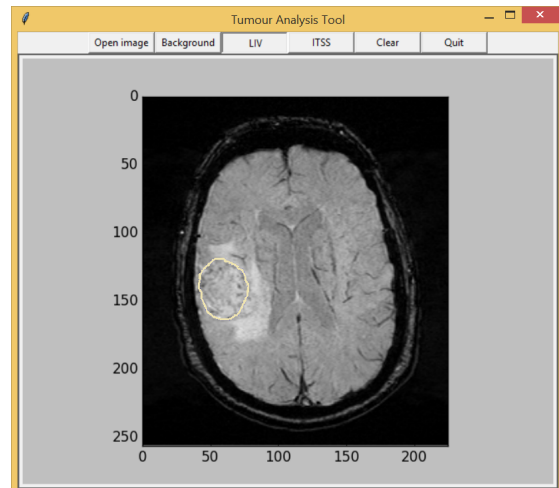


Figure 4.5: The user draws a region of interest and presses *LIV*.

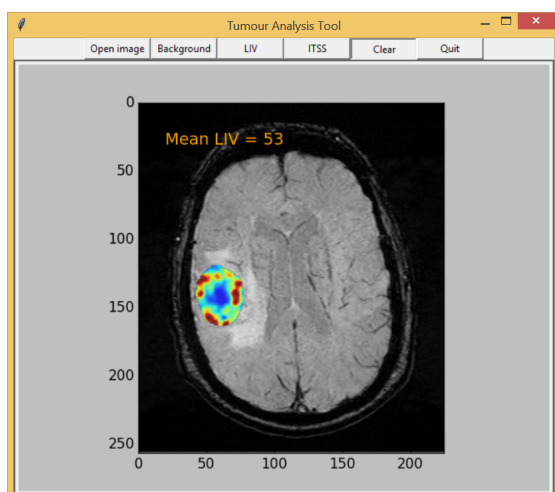


Figure 4.6: The LIV is presented. The user presses *Clear* to clear the numbers and coloured ROI and then *ITSS* to see the ITSS.

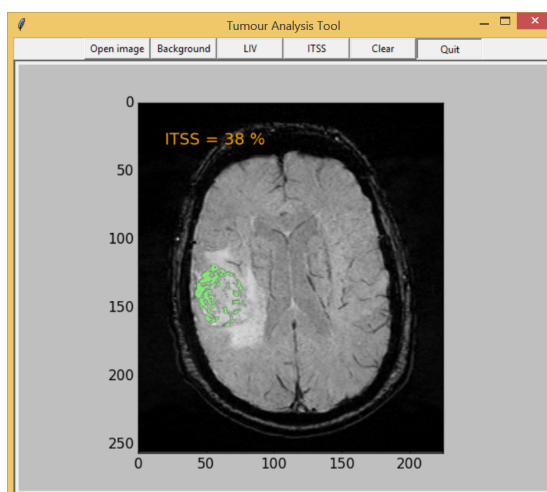


Figure 4.7: The ITSS is presented. To quit the program the user presses *Quit*.

4.1.1 Libraries and Functions

The most important libraries and functions used in this program are presented in table 4.1 below.

Table 4.1: Description of libraries and functions used in the program.

Library	General description	Important functions and usage
<i>Tkinter</i> 8.6	Python's standard GUI-package that contains positioning and control of widgets.	<code>Frame</code> , <code>Button</code> , <code>Text</code> , <code>Canvas</code> are some widgets used to build the GUI.
<i>NumPy</i> 1.9.2	Handles large multidimensional arrays and contains functions for operations on these.	Used for all array handling. <code>std</code> , <code>amin</code> , <code>amax</code> finds standard deviation, min and maximum values of an array.
<i>pydicom</i> 0.9.9	Reads, modifies and writes DICOM files.	Used to read and open DICOM files and extract data.
<i>matplotlib</i> 1.4.3	A plotting library that produces figures. Handles <i>NumPy</i> arrays.	Plots images and presents data. <code>LassoSelector()</code> is used to draw the ROIs. It is always active in the main loop and saves indices of the ROI and passes them to a callback function. <code>FigureCanvasTkAgg</code> embeds the plots from <i>matplotlib</i> into <i>tkinter</i> -GUI.
<i>SciPy</i> 0.15.1	Builds on the <i>NumPy</i> array object and contains modules for signal and image processing.	<code>gaussian.filter</code> from the subpackage <i>ndimage</i> convolves the image with a Gaussian filter.
<i>Mahotas</i> 1.3.0	For computer vision and image processing.	<code>thresholding.otsu</code> finds Otsu's threshold of an image.

4.2 Algorithm Description

`sigma` is the spread of the Gaussian function, σ , from equation 2.3 and `ncthresh` is the threshold value for the normalized contrast from section 2.5. Both `sigma` and `ncthresh` are defined in the beginning of the code. In the current stage the program demands that the user knows how it is working, there is no information text. A description of the image analysis algorithms is given in the following sections.

4.2.1 Finding Local Image Variance

The local image variance is found according to equation 2.2. It is displayed as a layer on top of the original image. The pixels of the image are rescaled to a value between 0 and 100 to avoid bias from difference in intensity ranges. The pseudo code is seen in the following list.

1. Rescale image.
2. Set corner elements outside ROI but inside matrix to zero.
3. Blur the part of the image that includes the chosen region of interest, `img_small` and `img_small`² using Gaussian filter function.
4. Find variance of each pixel according to equation 2.2.
5. Find mean of variance.
6. Display non-zero elements and mean on top of old image by updating canvas and text.

4.2.2 Finding Intratumoural susceptibility signal

The intratumoural susceptibility signal is found by first finding Otsu's threshold as explained in section 2.5. It is displayed as a layer on top of the original image and the pseudo code is seen in the following list.

1. Save background and standard deviation.
2. Set corner elements outside ROI but inside matrix to zero.
3. Divide non-zero elements into groups with Otsu's thresholding method.
4. Find mean of brighter group.
5. Find normalized contrast NC according to equation 2.8.
6. For $NC > ncthresh$
 - (a) Set pixels some colour.
7. Find part of image above threshold.
8. Display percentage and ITSS-structures on top of old image by updating canvas and text.

4.3 Analysing Local Image Variance

4.3.1 Filter parameters

In the study of local image variance by Grabner et al. Gaussian filter kernel with $FWHM = 3\text{mm}$ was used [6], corresponding to $\sigma = 1.3$ according to equation 2.7. This was done for another field strength and spatial resolution. For 1.5T as in this test the optimal filter parameters had to be determined to match the current resolution about $0.90 \times 0.90 \times 2\text{mm}$, seen in table 3.1.

In figure 4.8 that difference is shown as a function of truncation, for all different σ . The standard deviations (of $HG_{mean} - LG_{mean}$) are the errorbars plotted for each point. A higher σ shows a higher

distinction between HG and LG. This behaviour is same for all truncations but after a truncation of 2 pixels all groups look about the same. Therefore a truncation of 2 pixels is chosen as optimal.

Remember that the standard deviation mentioned here is the standard deviation of the mean local image variance of all the tumours in the HG and the LG-groups respectively. σ is the standard deviation of the Gaussian filter used. For different σ it is seen in figure 4.8 that both the difference and its standard deviation increase the larger the σ . The goal is to find as large difference as possible but as small standard deviation as possible. $\sigma = 2$ is chosen as a compromise from figure 4.8.

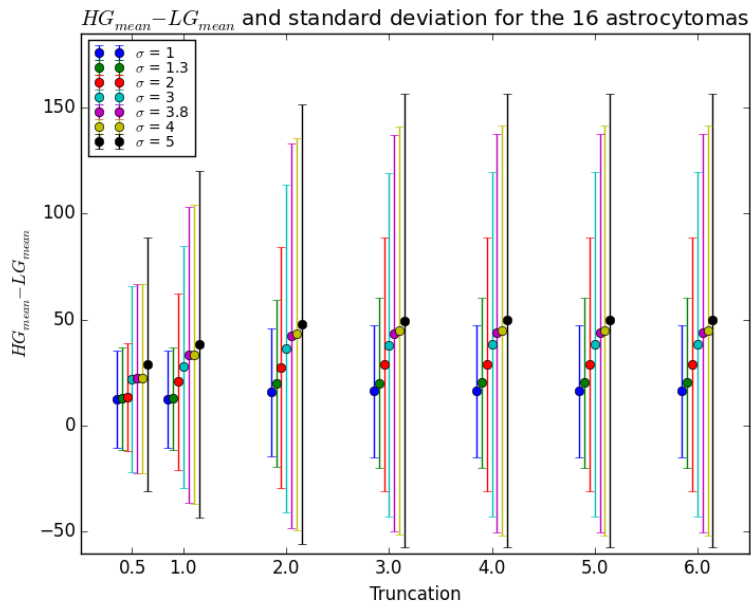


Figure 4.8: $HG_{mean} - LG_{mean}$ as a function of truncation and σ for the 16 gliomas.

However, two of the 16 patients were scanned at 3T (Siemens TrioTim) at a higher resolution. These patients have to be removed from the cohort since the variance is not representative when varying the field strength. Two tumours were oligodendroglioma which often are calcified. As explained in section 2.3 calcification shows as dark areas in SWI and can therefore be confused with hemorrhage or veins. One tumour was a pleomorphic xanthoastrocytoma, a very unusual tumour [9], that also contained parts of oligodendroglioma. So these three patients were also removed from the cohort. Left were four patients with astrocytoma grade II, one patient with anaplastic astrocytoma grade III and six patients with glioblastoma grade IV. One patient had a part of the tumour that clearly could be distinguished as hemorrhage (confirmed by CT), and that part had to be excluded when drawing the ROI. When removing these five special cases only the astrocytic tumours scanned at 1.5T are left and figure 4.9 shows the difference of $HG_{mean} - LG_{mean}$ for those. Note the different ranges on the y-axis when comparing figure 4.8 to 4.9. The standard deviation is clearly lower when analysing only the astrocytomas. As in figure 4.8 a truncation of 2 pixels seems to be optimal. $\sigma = 2$ is chosen again as a compromise between high differentiation between HG and LG and as low standard deviation as possible. The p-values were tested versus the truncation and σ , and the best results were achieved with this combination of $\sigma = 2$ and a truncation of two pixels.

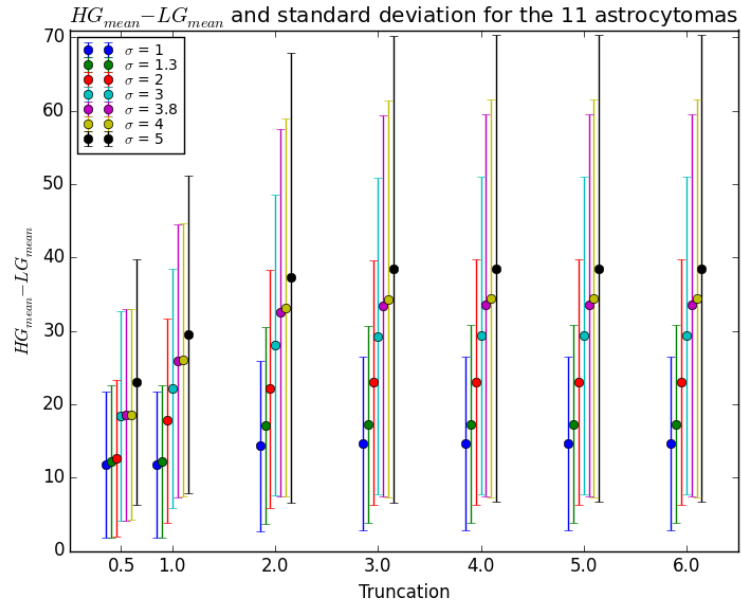


Figure 4.9: $HG_{mean} - LG_{mean}$ as a function of truncation and σ for the 11 astrocytomas

4.3.2 Test Results

The mean LIV versus the tumour grade for the 16 gliomas and the 11 astrocytomas is seen in figure 4.10. The mean and standard deviation when dividing the tumours into HG and LG groups can be seen in table 4.2. $p < 0.16$ means that no significant difference between the HG and LG group can be seen for the 16 gliomas. The Spearman correlation coefficient when correlating LIV for the 16 tumours to tumour grade was $r = 0.53$, $p < 0.04$. For the 11 astrocytomas $p < 0.03$ is significant for differentiating the means of the HG and LG groups. In that case Spearman correlation also show a significant correlation between mean LIV and tumour grade with values $r = 0.84$ and $p < 0.01$.

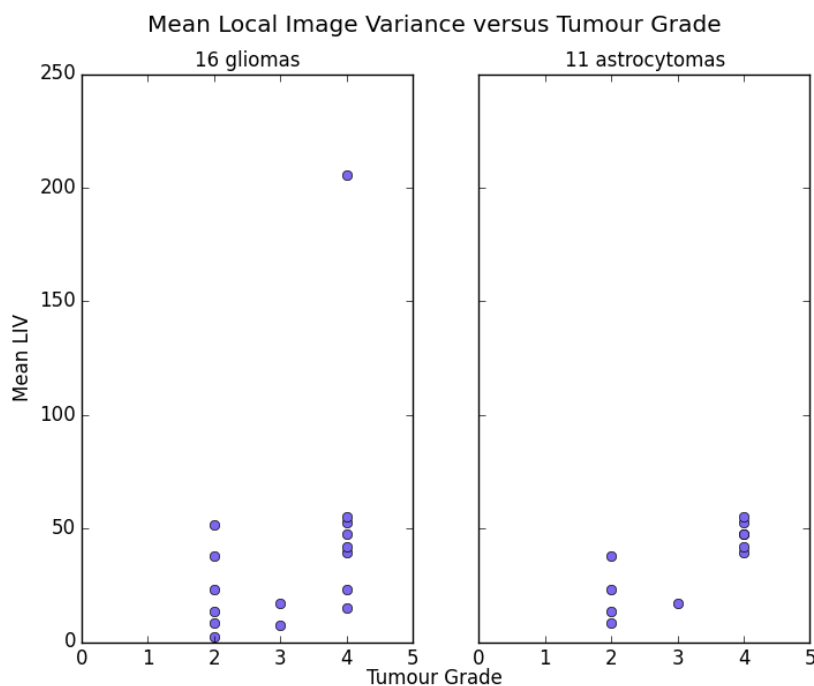


Figure 4.10: The mean local image variance versus tumour grade for all 16 gliomas and the 11 astrocytomas.

Table 4.2: The mean and standard deviation of LIV in the 16 gliomas and the 11 astrocytomas respectively.

Variable	16 gliomas	11 astrocytomas
LG_{mean}	23 (17)	21 (11)
HG_{mean}	50 (54)	43 (12)
$Total_{mean}$	40 (46)	35 (16)
$z - value$	-1.41	-2.27
$p - value$	< 0.16	< 0.03

4.3.3 Discrimination

To discriminate between the two groups of tumours a threshold value has to be set. This threshold value was found by looking at the statistics of the results above. Figure 4.11 shows boxplots of the results of the HG and LG groups, with first and third quartile of the values, including the median. The dashed line represents the spread of the data and the crosses are outliers. The small square represents the mean of the data. For all 16 gliomas no threshold could be set since the p-value showed no significance. For the 11 astrocytomas an appropriate threshold is set at a mean LIV level of 39. A mean LIV above 39 should therefore be a high grade tumour, and a mean LIV below should be a low grade tumour. The sensitivity and specificity are 86% and 100% respectively, according to equations 2.9 and 2.10.

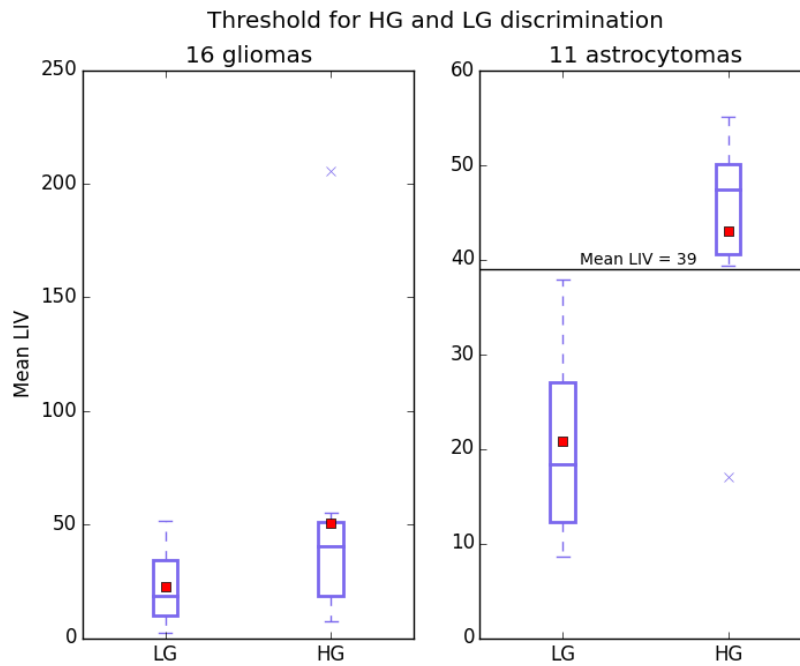


Figure 4.11: A boxplot of the results of the HG and LG groups, with first and third quartiles and their median. The square is the mean of the values. The horizontal line represents the threshold level for the 11 astrocytomas.

4.4 Intratumoural Susceptibility Signal

4.4.1 Threshold of Normalized Contrast

The p-values of discriminating the level of ITSS in the two groups are plotted versus the threshold of the normalized contrast (NC) in figure 4.12. The p-value of ITSS is lowest at a NC threshold of 12 ($p < 0.02$) for the 16 tumours and 14 ($p < 0.02$) for the 11 tumours. As can be seen, the values fluctuate between a threshold of 2-20, more for the astrocytomas than all the gliomas. As the threshold increases the values increase further, and an optimal NC threshold of 13 is chosen.

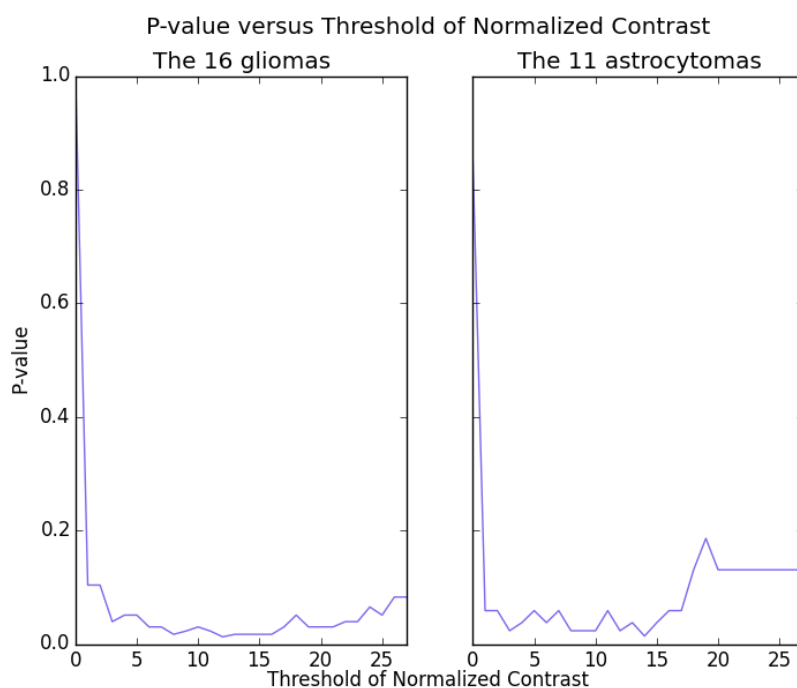


Figure 4.12: *P-values for the differentiation of HG and LG for the 16 gliomas and the 11 astrocytomas.*

4.4.2 Test Results

The intratumoural susceptibility signal versus the tumour grades for the 16 gliomas and the 11 astrocytomas is seen in figure 4.13. The mean and standard deviation when separating the tumours into LG and HG groups can be seen in table 4.3. $p < 0.02$ and $p < 0.04$ means that a significant difference between the groups can be seen for both the 16 gliomas and the 11 astrocytomas. Spearman correlation coefficients when correlating ITSS to tumour grade for the 16 gliomas were $r = 0.69$ and $p < 0.01$ and for the 11 astrocytomas $r = 0.63$ and $p < 0.04$.

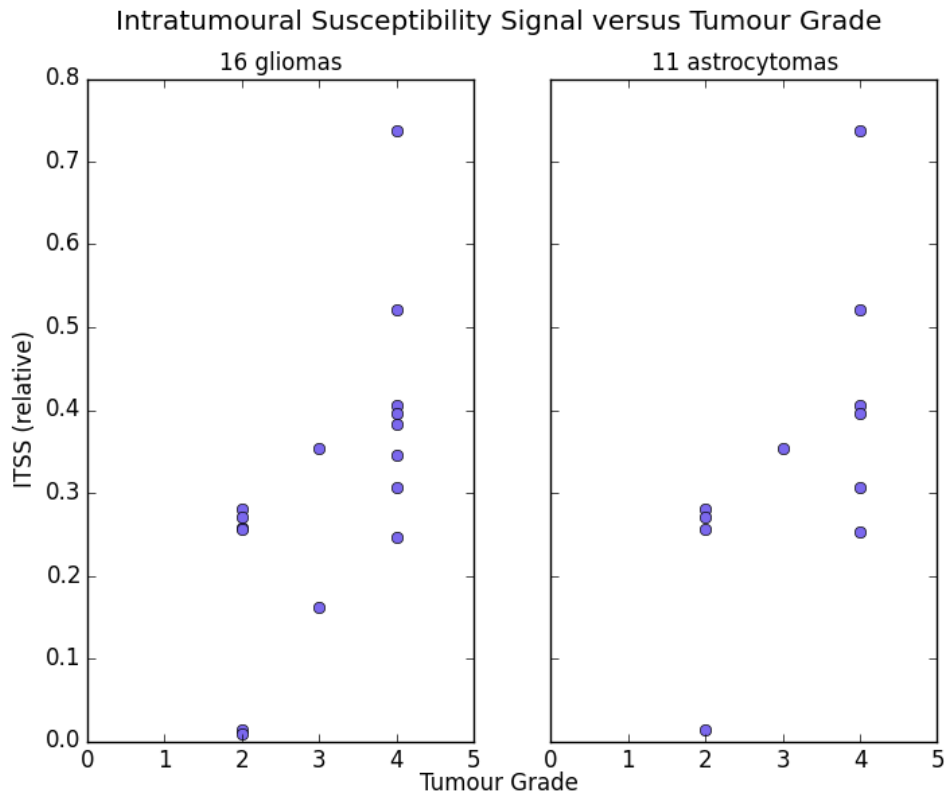


Figure 4.13: The intratumoural susceptibility signal versus tumour grade for all 16 gliomas and the 11 astrocytomas at a NC threshold of 13.

Table 4.3: The mean and standard deviation of ITSS in the 16 gliomas and the 11 astrocytomas respectively.

Variable	16 gliomas	11 astrocytomas
LG_{mean}	0.18 (0.12)	0.21 (0.11)
HG_{mean}	0.39 (0.15)	0.42 (0.15)
$Total_{mean}$	0.31 (0.17)	0.35 (0.17)
$z - value$	-2.39	-2.08
$p - value$	<0.02	<0.04

4.4.3 Discrimination

For a NC threshold of 13 the mean and the standard deviation when dividing the tumours into HG and LG groups is seen in table 4.3. A threshold level between the groups has to be set and this was done by looking at figure 4.14. A boxplot shows the first and third quartiles and the median. The dashed line represents the spread and the crosses are outliers. The small square represents the mean of the two groups. A threshold level of ITSS at 0.29 is set for both the 16 gliomas and the 11 astrocytomas. This yields a sensitivity and specificity of 80% and 100% respectively for the 16 gliomas and 86% and 100% respectively for the 11 astrocytomas according to equations 2.9 and 2.10.

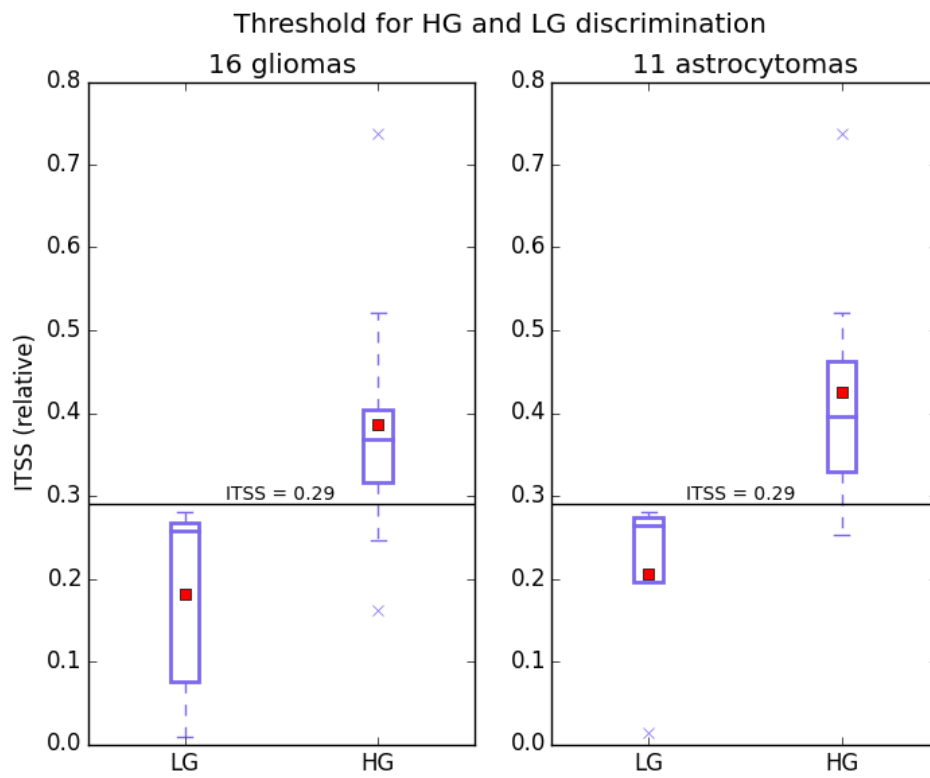


Figure 4.14: A boxplot of the ITSS results of the HG and LG groups. The small square is the mean of the values. The horizontal lines represent the threshold level for discriminating between the two groups.

Chapter 5

Discussion

This section elaborates further on the results and connects them to the research in the field. The first focus is on the program and the algorithm. Then the results of the image analyses are discussed, before some general thoughts about the method for segmenting the tumours and future work.

5.1 The Program

An advantage of developing a program in *Python* is that it is open and free. It has an extensive standard library and the source code for all algorithms can be viewed and studied when there is a doubt about how something is computed, for example the Gaussian filter function in this program. The program can easily be transferred to an exe-file that can be opened by the radiologists at any PC. For Ubuntu the file need to be run through Wine.

The software program should be quite intuitive. If an error is made the program does not crash but nothing happens. For example opening a file in wrong file format raises no error but the image does not load. An option would be to add a dialogue box telling the user to choose a DICOM file. If the user forgets to press `Clear` before making a second analysis the numbers presenting LIV and ITSS get stuck on the screen until the program is restarted. The colour representation of LIV and ITSS can always be cleared afterwards.

5.2 Filtering

A limitation of this study is the corner handling when doing the Gaussian filtering in the LIV analysis. Figure 5.1 shows a tumour with a hemorrhage. The ROI (red curve) excludes the hemorrhage, the dark spot next to the upper right corner of the ROI. Figure 5.2 shows how the Gaussian filter handles these kind of edges. The red circle is still the same segmented ROI. The grey box around it is the bounding box, the matrix picked out for analysis. The white boxes are the central elements around which a Gaussian blur is made. The dashed boxes are the pixels that contribute when calculating this Gaussian blur of each central element. A truncation of two pixels means that two pixels next to the central element contributes to the Gaussian blur. At the edges that are closer than two pixels away from the edges of the bounding box, the pixels contributing to the blur are reflected from the matrix within the bounding box. At the edges that are not restricted by the bounding box it is the truncation that limits the averaging. Thus, if a hemorrhage (or other intense region) is close enough to this kind of edge it can contribute to raise the mean LIV. This can be observed in figure 5.2, more clearly in the vertical direction. Dark spots from the hemorrhage outside the upper right corner contribute in the second element. Another approach would have been to restrict the analysis to the area two pixels away from the edges. This was not done since some ROIs were quite narrow and consisted of only a few pixels. Choosing a truncation of two pixels reduce this dependence of the geometrical location of the tumour. As could be observed in the results in figures 4.8 and 4.9 increasing the truncation did not lead to a better differentiation between the LG and HG group.

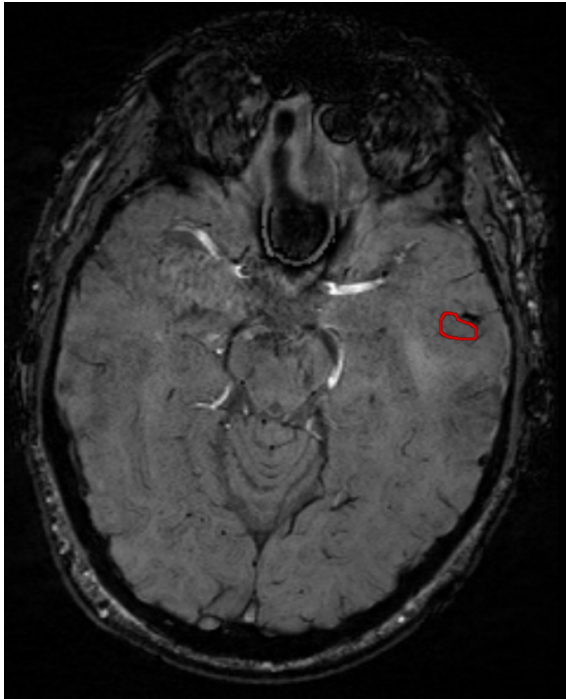


Figure 5.1: *The most malignant part of a tumour. Hemorrhage can be seen at the top right corner outside the ROI.*

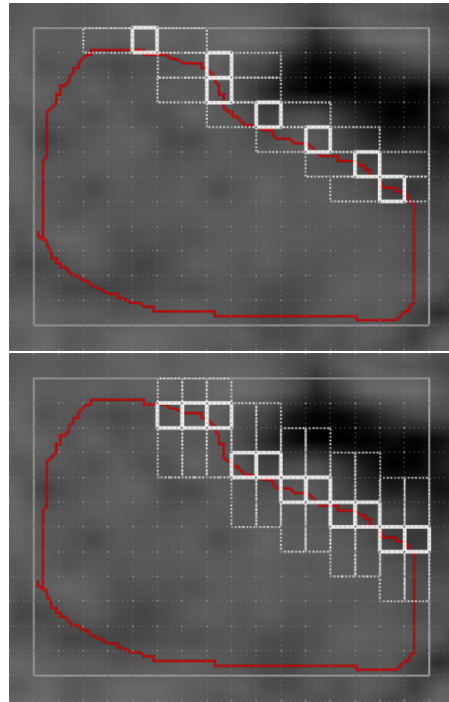


Figure 5.2: *The elements that contribute in the edge handling by the Gaussian filter used, in the horizontal and vertical direction respectively.*

The Gaussian filter function implemented in *SciPy* is a combination of 1D-filters, run in each direction. The research by Grabner et al. does not state the exact implementation of the filter used and this might be a reason for different results [6].

5.3 Local Image Variance

The local image variance for all gliomas did not correlate significantly to the glioma grade ($p < 0.16$). This was due to the fact that susceptibility-weighted magnitude images not only represents blood vessels but also hemorrhage and calcification. This has already been highlighted in other studies [5, 4], so another approach was to exclude the tumours with high calcification and to exclude the obvious hemorrhage from the regions of interest. This can be done on the basis of low signal in conventional MRI and SWI phase imaging. So in this project the 11 astrocytomas were also studied separately. The results were that the mean of the mean LIV could be distinguished between the two groups ($p < 0.03$). The study by Grabner et al. showed significant results for glioma (and not the subgroup astrocytoma) but does not state the specific tumours in the study [6], so if it includes oligodendroglioma or not remains unknown. According to this study there is a difference in evaluating astrocytoma and oligodendroglioma.

For the local image variance analysis Grabner et al. had a field strength of 7T, compared to 1.5T in this project [6]. The scanner parameters can be seen in table 5.1. The difference in resolution is about a factor 3, and 7T make small susceptibility differences easier to distinguish and the resulting variance should be larger. The higher resolution lead to a wider range of values (for Grabner et al. typically in the range of 0-350) which should make it easier to separate the values into two groups with different means. In this study the LIV-values were in the range of 0-55, with an outlier (due to large hemorrhage) at 206. Discriminating the two groups is a relative measurement but the outliers are probably better handled in the test by Grabner et al. The smallest microvessels (capillaries) are about 5-10 μm and cannot be seen a 1.5T. Signals for voxels that contain mixed tissues, partial volume effects, will be greater for the 1.5T-scanner since the voxels are larger. The signal is the average of the signal from the tissues inside the voxel and a

higher resolution will give a more correct representation of the variance.

Table 5.1: *The parameters used in the study by Grabner et al. [6] and the parameters from this study.*

Parameters	Grabner et al.	This project
Scanner	Siemens	Siemens
Field strength (T)	7	1.5
TE (ms)	15	40
TR (ms)	28	49
Image matrix (pixels)	704 x 704	256 x 224
Resolution (mm)	0.3 x 0.3 x 1.2	0.9 x 0.9 x 2.0

5.4 Intratumoural Susceptibility Signal

In other studies the "small linear or dot-like lesions" of ITSS were segmented manually [5, 4]. In the study by Chuang et al. the hypointense areas were distinguished automatically by a computer program, but a whole volume was studied and the volumetric percentage for the whole tumour in three dimensions was calculated [7]. A standard deviation of the signal in white matter was used as denominator in equation 2.8, to represent the signal fluctuation [7]. This could be done since they computed their regions in a volume and always had a possibility to find white matter. In this study only one slice of the tumour has been selected, therefore the fluctuation of the signal was instead found by computing the standard deviation of a background ROI in the dark upper left corner of the image, after checking that there were no artefacts present. This gave rise to a different standard deviation than the one used by Chuang et al. which naturally implies another threshold for the normalized contrast and grade discrimination. The scanner parameters in the study by Chuang et al. are seen in table 5.2. The field strength was the same as in this study but the image matrix was much larger. All other ITSS studies have focused on astrocytomas rather than all gliomas [5, 4, 7], and for reasons mentioned above as calcification and hemorrhage this seems more reasonable. The results of this study however show $p < 0.02$ for all gliomas and $p < 0.04$ for the 11 astrocytomas, which is statistically significant. This is consistent with the studies of Park et al. and Wang et al. which however exclusively focuses on astrocytoma [4, 5]. One study uses the word "gliomas" in the title, but only includes diffuse astrocytomas in the method [4].

Table 5.2: *The parameters used in the study by Chuang et al. [7] and the parameters from this study.*

Parameters	Chuang et al.	This project
Scanner	GE Healthcare Signa HDx	Siemens
Field strength (T)	1.5	1.5
TE (ms)	39	40
TR (ms)	50	49
Image matrix (pixels)	512 x 512	256 x 224
Resolution (mm)	0.6 x 0.5 x 2.5	0.9 x 0.9 x 2.0

5.5 General

When segmenting the tumours the regions of interest (ROIs) were selected as the most malignant part of the tumour. The ROI was selected where a hole from resection could be seen in a later examination, to be sure to analyse the area that corresponded to the tissue sample. In the analyse of the 11 astrocytomas only, macrohemorrhage was excluded where it could be seen. In some cases up to eleven samples had been taken at the same biopsy, and the microscopical analysis showed different grades. A tumour consisting of several grades should be classified as the most malignant part and consequently it is important to draw the ROI at that part specifically. Sometimes the biopsy was taken a few months after the image analysed in this

study, this may have changed the disease profile.

One limitation of this study was the small number of patients. Particularly the number of LG patients was very low, six in the analysis of all gliomas and four when the study was limited to astrocytomas. A small number of LG patients compared to the HG group is commonly occurring in most research studied during this project [7, 19], and is in this case due to the fact that most low grade tumours do not get a biopsy and treatment directly. The changes in the tumourous tissue are instead observed and kept track of, as they can evolve into a more malignant tumour over the years. Thus, it is hard to find patients with a confirmed tumour of grade I and also of grade II. There are other factors than biopsy that determine the characteristics of a tumour, for example the location, and it is always necessary to consider the whole clinical image before diagnosing.

Susceptibility-weighted images are hypointense both at regions consisting of blood products as well as calcified regions, which make them impossible to separate. This is why the oligodendroglioma were removed from the study, since they generally contain a lot of calcification. The SWI-phase image can however distinguish between the two, since a diamagnetic structure (such as calcium) repels the magnetic field, as opposed to a paramagnetic structure (such as deoxyhemoglobin) that aligns with the field. Calcification and blood products are seen in separate colours (depending on manufacturer, for example Siemens left handed system show calcification as black and hemorrhage as white). For clinical use it would thus be evident that the neuro-radiologists make more use of the SWI-phase image.

Since this study is retrospective and the images are obtained at different scanners with embedded filters, their reconstructions are all different and might contribute to errors when comparing the images. In the ideal case one would have exactly the same filter and protocol for all scanners, when doing a multi-site study like this. If the *Tumour Analysis Tool* were to be used clinically there would have to be a standard discrimination level for each scanner, for example field strengths and resolutions should never be mixed.

The largest limitation of this project was the small patient cohort, and more patients and images are needed to get a reliable result. Another thing that remains to be tested is the intraobserver consistency as the tumours in this study were segmented by only one neuro-radiologist.

5.6 Future

Other image processing techniques show other correlations to grade, for example perfusion-weighted imaging with dynamic contrast enhancement. A combination of these could lead to a perfect grading of the tumours. With a higher field strength it might even be possible to discriminate grade III from grade IV.

The code in the program can be extended to take other analyses as well, but the first thing to do would be to close the loopholes talked about in section 5.1, by adding a few user friendly dialogue boxes or some information text.

The *Tumour Analysis Tool* implemented outputs the mean local image variance and the degree of intra-tumoural susceptibility signal. In future work it would be interesting to display the tumour grade directly and state the certainty of the analysis. To do and get reliable basic data more tumours have to be analysed.

Chapter 6

Conclusion

The *Tumour Analysis Tool* is a computer program with a graphical user interface where a radiologist can open a DICOM image and draw a ROI. The ROI can be analysed with respect to local image variance (LIV) and the intratumoural susceptibility signal (ITSS). The software outputs the level of mean LIV and ITSS computed with the predefined Gaussian filter parameters and NC -threshold value based on the 16 tumours studied in this project. The construction of the code easily admits other types of analyses to be implemented.

The mean LIV seems to be useful for discriminating between high and low grade astrocytomas, but not gliomas in general, when excluding the obvious hemorrhages. ITSS is able to discriminate between the groups of high and low grade gliomas. The results of the image analyses are consistent with other research in the field. Thus, the *Tumour Analysis Tool* could be a help for the radiologists when separating glioma into high and low grade. Still, the calcification and hemorrhage always need to be taken into consideration and excluded with help from other images such as CT and contrast enhanced T_1 -weighted MR-images.

The results of this project indicate that the *Tumour Analysis Tool* is useful for determining tumour grade from SWI-images but the program remains to be tested on a larger cohort and by more radiologists.

Chapter 7

Bibliography

- [1] M.K.L. Goodenberger and R.B. Jenkins. Genetics of adult glioma. *Cancer genetics*, 205(12):613–621, 2012.
- [2] A. Drevelegas. *Imaging of brain tumors with histological correlations*. Springer Science & Business Media, 2010.
- [3] V. Sehgal, Z. Delproposto, E.M. Haacke, K.A. Tong, N. Wycliffe, D.K. Kido, Y-B. Xu, J. Neelavalli, D. Haddar, and J.R. Reichenbach. Clinical applications of neuroimaging with susceptibility-weighted imaging. *Journal of Magnetic Resonance Imaging*, 22(4):439–450, 2005.
- [4] M.J. Park, H.S. Kim, G-H. Jahng, C-W. Ryu, S.M. Park, and S.Y. Kim. Semiquantitative assessment of intratumoral susceptibility signals using non-contrast-enhanced high-field high-resolution susceptibility-weighted imaging in patients with gliomas: Comparison with mr perfusion imaging. *American Journal of Neuroradiology*, 30:1402–1408, 2009.
- [5] X-C. Wang, H. Zhang, Y. Tan, J-B. Qin, Z-F. Wu, L. Wang, and L. Zhang. Combined value of susceptibility-weighted and perfusion-weighted imaging in assessing who grade for brain astrocytomas. *Journal of Magnetic Resonance Imaging*, 39:1569–1574, 2014.
- [6] G. Grabner, S. Goed, A. Wöhrer, C. Marosi, A. Mert, S. Wolfsberger, G. Widhalm, S. Trattinig, and M. Preusser. Quantification of 7 Tesla hypointensities in gliomas using the local image variance. Study presented at ESMRMB Conference in Vienna 2014.
- [7] T-C. Chuang, W-P. Shui, H-W. Chung, and P-H. Lai. Quantitative intra-tumoral susceptibility signal in grading brain astrocytomas with susceptibility-weighted imaging. Study presented at Annual Meeting of International Society of Magnetic Resonance in Medicine, Milan, Italy, 2014.
- [8] G.M. Cooper. *Elements of human cancer*. Jones & Bartlett Learning, 1992.
- [9] M.F. Reiser, W. Semmler, and H. Hricak. *Magnetic Resonance Tomography*. Springer-Verlag Berlin Heidelberg, 2008.
- [10] Q.T. Ostrom, H. Gittleman, P. Liao, C. Rouse, Y-W. Chen, J. Dowling, Y-L. Wolinsky, C.Kruchko, and J. Barnholtz-Sloan. Cbtrus statistical report: primary brain and central nervous system tumors diagnosed in the united states in 2007–2011. *Neuro-oncology*, 16(suppl 4):iv1–iv63, 2014.
- [11] D.W. McRobbie, E.A. Moore, M.J. Graves, and M.R. Prince. *MRI from Picture to Proton*. Cambridge University Press, University Printing House, Cambridge CB2 8BS, United Kingdom, 2007.
- [12] R.F. Józefowicz. Department of Neurology University of Rochester. Axial MRI - t1 vs. t2. <http://www.urmc.rochester.edu/libraries/courses/neuroslides04/other/images/016.png>. 2015-05-26.
- [13] E.M. Haacke, S. Mittal, Z. Wu, J. Neelavalli, and Y-CN. Cheng. Susceptibility-weighted imaging: technical aspects and clinical applications, part 1. *American Journal of Neuroradiology*, 30(1):19–30, 2009.
- [14] A. Rovira. SWI in neurological disorders. ESMRMB Conference, November 2014.
- [15] K.A. Tong, S. Ashwal, A. Obenaus, J.P. Nickerson, D. Kido, and E.M. Haacke. Susceptibility-weighted MR imaging: a review of clinical applications in children. *American Journal of Neuroradiology*, 29(1):9–17, 2008.

CHAPTER 7. BIBLIOGRAPHY

- [16] N. Otsu. A threshold selection method from gray-level histograms. *Automatica*, 11(285-296):23–27, 1975.
- [17] Wikipedia. Otsu’s method. <https://en.wikipedia.org/wiki/otsu>. 2015-08-10.
- [18] A.L. Strömvall. Images and image processing. Lecture in course Physics of X-rays, Umeå University, 2013.
- [19] S. Trattnig. Clinical applications at 7T. ESMRMB Conference, November 2014.